

A MASSIVE-STAR FORMING INFRARED LOOP AROUND THE CRAB-LIKE SUPERNOVA REMNANT G54.1+0.3: POST MAIN-SEQUENCE TRIGGERED STAR FORMATION?

BON-CHUL KOO¹, CHRISTOPHER F. MCKEE², JAE-JOON LEE³, HO-GYU LEE¹, JEONG-EUN LEE⁴, DAE-SIK MOON⁵, SEUNG SOO HONG¹, HIDEHIRO KANEDA⁶, AND TAKASHI ONAKA⁷

Draft version October 28, 2018

ABSTRACT

We report the discovery of a star-forming loop around the young, Crab-like supernova remnant (SNR) G54.1+0.3 using the *AKARI* infrared satellite. The loop consists of at least 11 young stellar objects (YSOs) embedded in a ring-like diffuse emission of radius $\sim 1'$. The YSOs are bright in the mid-infrared and are also visible in the *Spitzer* Space Telescope Galactic plane survey images. Their *Spitzer* colors are similar to those of Class II YSOs in [3.6]–[5.8] but significantly redder in [8]–[24], i.e., $0 < [3.6] - [5.8] < 1.2$ and $5 < [8] - [24] < 9$. Most of them have near-infrared counterparts in the 2MASS *JHK_s* images, and some of them have an optical counterpart too. Their *JHK_s* colors and magnitudes indicate that the YSOs are massive ($\gtrsim 10 M_{\odot}$) pre-main-sequence stars at the same distance to the SNR, i.e., 8 kpc, which supports the association of the star-forming loop with the SNR. The dereddened spectral energy distributions are similar to *early* Herbig Be stars, which are early B type pre-main-sequence stars with inner disks that have been destroyed. The confinement to a loop structure indicates that the YSOs are young, i.e., $\lesssim 2$ Myr. We propose that their formation is triggered by the progenitor star of G54.1+0.3, which has a mass of $\lesssim 15 M_{\odot}$. The triggering must have occurred near the end of the progenitor's life, possibly after it had evolved off the main sequence.

Subject headings: ISM: individual (G54.1+0.3) — infrared: stars — stars: formation — stars: pre-main-sequence — supernovae: general — supernova remnants

1. INTRODUCTION

Massive stars can trigger the formation of a next generation of stars. Their strong stellar ultraviolet radiation and winds can compress the ambient medium so that it becomes gravitationally unstable and collapses. Numerous examples supporting the scenario of triggered star formation have been proposed, from young stars formed in small bright-rimmed globules inside HII regions to OB associations around kiloparsec supershells (see Elmegreen 2002; Zinnecker & Yorke 2007, and references therein).

In this Letter, we report the discovery of a unique example of triggered star formation, namely triggering by the progenitor star of a young, core-collapse SNR. The SNR (G54.1+0.3) is Crab-like, with centrally-brightened synchrotron emission in radio and X-rays (Velusamy & Becker 1988; Lu et al. 2002). The extent of the remnant is $120'' \times 80''$ and is much fainter than the Crab, e.g., 0.5 Jy versus 1040 Jy at 1 GHz. At the center, a 136 ms radio/X-ray pulsar with a characteristic age of 2900 yr has been discovered (Lu et al. 2002). The

distance to the SNR is 8 kpc (§ 4). This object provides a laboratory in which to explore the physics of triggered star formation.

2. DISCOVERY OF THE IR LOOP

A mid-infrared (MIR) observation of G54.1+0.3 was done using the Infrared Camera (IRC) aboard *AKARI* on 2007 April 17. The observation was performed in a framework of the *AKARI* mission program: the ISM in our Galaxy and nearby galaxies (ID: 1401070.1, PI: H.K.) The IRC is equipped with three wave band channels covering the 2.6–26 μm wavelength range with a $10' \times 10'$ field-of-view (FOV) (Onaka et al. 2007). We used the MIR-L channel in IRC02 mode, which gave two band images, L15 and L24, centered at wavelengths of 15.58 and 22.89 μm , respectively. Their angular resolutions are $5.''7$ (L15) and $6.''8$ (L24). The total on-source integration time was 196 s for each band. The basic calibration and data handling were processed using the standard IRC Imaging Data Reduction Pipeline version 070104⁸. The positional uncertainty is $0.''15$ at the 1- σ confidence level.

Fig. 1 shows the *AKARI* L15 image of G54.1+0.3 with the 4.85 GHz radio continuum image overlaid. The radio image was made from archive data of the Very Large Array (VLA) of the National Radio Astronomy Observatory⁹; the data were originally obtained by Velusamy & Becker (1988). The *AKARI* image shows a well-defined, bright, ring-like structure at the posi-

¹ Department of Physics and Astronomy, Seoul National University, Seoul 151-742, Korea; koo@astrohi.snu.ac.kr, hglee@astro.snu.ac.kr, sshong@astro.snu.ac.kr

² Department of Physics and Astronomy, University of California, Berkeley, CA94720, USA; cmckee@astro.berkeley.edu

³ Astronomy & Astrophysics Department, Pennsylvania State University, University Park PA16802, USA; lee@psu.edu

⁴ Department of Astronomy and Space Science, Sejong University, Seoul 143-747, Korea; jelee@sejong.ac.kr

⁵ Department of Astronomy & Astrophysics, University of Toronto, Toronto ON M5S 3H4, Canada; moon@astro.utoronto.ca

⁶ Institute of Space and Astronautical Science, JAXA, Kanagawa 229-8510, Japan; kaneda@ir.isas.jaxa.jp

⁷ Department of Astronomy, University of Tokyo, Bunkyo-ku, Tokyo 113-0003, Japan; onaka@astron.s.u-tokyo.ac.jp

⁸ <http://www.ir.isas.jaxa.jp/ASTRO-F/Observation/DataReduction/IRC/>

⁹ The National Radio Astronomy Observatory is a facility of the National Science Foundation operated under cooperative agreement by Associated Universities, Inc.

tion of the SNR (see also Slane 2007). The ring appears partially complete with its northeastern portion opened, with faint ridges extending out from the ends of the bright ring. The bright portion of the ring (hereafter the “main ring”) is elongated along the northwest-southeast direction and has an extent of $\sim 105'' \times 54''$, or 4.1×2.1 pc at 8 kpc. The ring is composed of both diffuse and compact sources. Most of the compact sources are point-like except the bright one at the northwestern end. There are more than 10 point sources distributed along the main ring and several others at the ‘tips’ of the faint ridges. Most of them are bright in the $24 \mu\text{m}$ image and have colors quite different from foreground/background stars. This can be seen in Fig. 1 (right), which is a three-color image produced from the *Spitzer* IRAC $5.8 \mu\text{m}$ (B), *AKARI* $15 \mu\text{m}$ (G), and *Spitzer* MIPS $24 \mu\text{m}$ (R) images. We obtained the *Spitzer* image of the source from the GLIMPSE (Galactic Legacy Infrared Mid-Plane Survey Extraordinaire, Release II) and MIPS GAL legacy projects. There are 11 sources with colors significantly redder than the other stars in the field (see also the inset in Fig. 2).

3. YOUNG STELLAR OBJECTS IN THE IR LOOP

We conducted photometry of a 4.5 -radius area surrounding the IR loop using the *AKARI* 15 and $24 \mu\text{m}$ and the *Spitzer* MIPS $24 \mu\text{m}$ and $70 \mu\text{m}$ images. We have identified 151 sources detected in at least one of the 15 or $24 \mu\text{m}$ bands; most of them were detected at $15 \mu\text{m}$ while 76% were detected at $24 \mu\text{m}$. At $70 \mu\text{m}$, only one source was identifiable and only upper limits are derived for the rest. The photometry of stars in the IR loop is not straightforward because of the bright diffuse emission from the loop. We did PSF photometry to minimize the contamination due to the diffuse emission. Sources are crossidentified with the *Spitzer* GLIMPSE catalog, which contains fluxes of the four IRAC bands, and also with the 2MASS Second Incremental Release Point Source Catalog.

Fig. 2 shows the *Spitzer* $[3.6]-[5.8]$ versus $[8]-[24]$ color-color plot of the 64 sources detected in the IRAC and MIPS $24 \mu\text{m}$ bands with a $[24]$ magnitude error of less than 0.2 mag. The stars clustered near (0.0, 0.0) are probably main-sequence or giant stars along the line of sight. The sources along the IR loop are well defined in this diagram by their strong $[8]-[24]$ excess and moderate or small $[3.6]-[5.8]$ excess, i.e., $5 < [8]-[24] < 9$ and $0 < [3.6]-[5.8] < 1.2$. The sources within this box are marked by filled circles. The half-filled circles with arrows in the box represent the sources not detected in one of the IRAC 5.8 and $8.0 \mu\text{m}$ bands but are included because they are likely to fall into the box based on their MIR colors. We marked their positions using a shorter IRAC band, e.g., if a source is not detected at $8.0 \mu\text{m}$ we used $[5.8]$ instead of $[8.0]$ and placed an arrow. The inset shows that all sources in the box are distributed along the IR loop, although the loop of YSOs is quite distorted. Their colors are different from those of previously studied YSOs in nearby star-forming regions. We show this by drawing boxes (dotted lines) in Fig. 2 representing the areas occupied by young embedded protostars with both circumstellar disks and envelopes (Class 0/I) and pre-main sequence stars with significant circumstellar disks (Class II) determined by previous studies (e.g.,

Muzerolle et al. 2004). It is clear that the YSOs in the IR loop do not fall into the usual Class 0/I or Class II areas and that this cannot be due to extinction. There are many sources that fall into and around Class II areas. They are outside the IR loop and will not be discussed further in this paper.

Fig. 3 (bottom) shows a $J-H$ versus $H-K_s$ color-color diagram for all 110 MIR sources identified in the 2MASS JHK_s bands. The small dots represent sources not detected in *Spitzer* MIPS $24 \mu\text{m}$ or IRAC bands while the other symbols have the same meaning as in Fig. 2. There are only nine filled/half-filled circles because two YSOs with large $[3.6]-[5.8]$ (Fig. 2) are not identified in the 2MASS bands. The dashed line represents the main-sequence (MS), which is from Bessel & Brett (1988) for stars later than A0 and is based on calculations of the JHK_s colors from Kurucz model atmospheres (Castelli & Kurucz 2003) for stars earlier than A0. The dotted line represents interstellar reddening line of an A0 star following the reddening law of Bessel & Brett (1988). Note that the YSOs are clustered around the positions of reddened OB stars. Another way to see this is from the color-magnitude (K_s vs. $H-K_s$) diagram (Fig. 3 top). In this diagram, the dashed line represents the MS at 8 kpc calculated from the Kurucz model atmospheres and using the relation between effective temperature and radius of MS stars. We adopt the relation of Martins, Schaerer, & Hillier (2005) for O-type stars and that of Schmidt-Kaler (1982) for stars later than B0. For B0 stars, we interpolate the two with an adopted temperature of $T_{\text{eff}} = 30,000$ K. The dotted lines represent the reddening lines that bound the YSOs. The YSOs are again clustered around the positions of reddened early-type stars. The YSOs are not aligned along a single MS line, but that may be due to slightly different amounts of extinction toward individual sources. The extinction toward individual objects can be derived if we assume that they are on the MS, and it ranges from $A_V = 6.9$ to 9.2 with a mean of $A_V = 8.0 \pm 0.7$ mag. The mean extinction agrees very well with the extinction implied from the X-ray absorbing H columns to the SNR, i.e., $A_V = 8.4 \pm 0.5$ mag from $N(H) = 1.6(\pm 0.1) \times 10^{22} \text{ cm}^{-2}$ (Lu et al. 2002). We conclude that the JHK_s color-color and color-magnitude diagrams are consistent with the YSOs being massive pre-main-sequence stars at 8 kpc. The spectral types determined from their K_s magnitudes in Fig. 3 (top) are B1.5 to O8, which have $T_{\text{eff}} = 23,000 - 35,000$ K, masses of $12-21 M_{\odot}$, and luminosities of $(1-10) \times 10^4 L_{\odot}$.

Fig. 4 shows the SED of the most luminous source in the K_s band (the brightest one in the southern part of the loop in Fig. 1) as an example of the YSO SEDs. The filled symbols represent dereddened fluxes using the value $A_V = 6.9$ mag derived from Fig. 3 and an interstellar reddening law with $R_V = 3.1$ (Draine 2003). The dereddened SED is characterized by a star-like SED with a MIR/FIR excess at $\gtrsim 8 \mu\text{m}$, as we could have inferred from Figs. 2 and 3. The spectrum at $\lesssim 5 \mu\text{m}$ matches reasonably well the SED of a 35,000 K MS star, the temperature of which was determined from its K_s magnitude (Fig. 3). This spectrum is quite similar to the SED of early Herbig Be (HBe) stars (spectral type B0-B5; group III) (Hillenbrand et al.

1992; Malfait, Bogaert, & Waelkens 1998). A dip at 6–10 μm similar to that in Fig. 4 was observed in HBe stars and has been interpreted as a physical hole in the dust distribution caused by the break-up of inner disks (Malfait, Bogaert, & Waelkens 1998). If we consider the MIR/FIR excess at $\gtrsim 8 \mu\text{m}$ to arise from an optically thick disk with a constant effective temperature and fit the SED with a 35,000 K star plus a blackbody, we obtain a disk with a temperature of 190 K and a luminosity of 160 L_{\odot} , although this fit is not quite satisfactory. Most YSOs in the IR loop have SEDs similar to Fig. 4, with some objects showing weak MIR excess also. The ratio of the disk to stellar luminosity is $\lesssim 1\%$, showing that there is not much circumstellar material near the YSOs. If we use the empirical relationship of Nakajima et al. (2005) between stellar masses and K magnitudes for group III HBe stars, the masses of the YSOs range from 12 to 18 M_{\odot} which agrees with our estimates above. The 2MASS survey has a limiting K_s -band sensitivity of 14.3 mag, corresponding to a 6 M_{\odot} star at 8 kpc with 8 mag of extinction; no additional MIR sources are seen between 13.2 and 14.3 mag in the vicinity of the IR loop, however, which suggests a non-standard IMF for this region.

4. SNR/IR LOOP ASSOCIATION AND THEIR DISTANCE

The IR loop surrounds the X-ray/radio bright central portion of the SNR almost perfectly. The SNR is somewhat extended along the northeast-southwest direction, suggesting that its expansion has been blocked toward the IR ring. We note that the radio contours are deformed around the northwest, which is consistent with encountering a dense medium there. The positional coincidence with a detailed spatial correlation strongly suggests that the IR loop and the SNR G54.1+0.3 are associated. The agreement between the extinction toward the IR loop and the X-ray absorbing column toward the SNR further supports the association (§ 3). The absence of direct evidence for the interaction of the SNR shock with the dense gas may be understood if we assume that the IR loop is a partial shell in a low density medium, so that the SNR shock has been able to propagate well beyond the loop now.

The distance to G54.1+0.3 has been determined by Camilo et al. (2002), who derived the dispersion measure of the central pulsar (308 $\text{cm}^{-3} \text{pc}$) and noted that it corresponded to a distance of 8–12 kpc, depending on the electron-distribution model of the Galaxy. We have obtained an HI absorption spectrum of the SNR using the VLA Galactic Plane Survey data (Stil et al. 2006). The HI spectrum of the SNR shows HI absorption over all positive velocities, which indicates that G54.1+0.3 is beyond the tangent point (≥ 5 kpc). The absorption peak occurs at +23 km s^{-1} , and at this velocity there is a faint $^{13}\text{CO } J = 1-0$ emission coincident with the IR loop in the Boston-University-Five College Radio Astronomy Observatory Galactic Ring Survey (Jackson et al. 2006). The emission is weak ($T_b \leq 0.7$ K) and implies a mass $\lesssim 400 M_{\odot}$. The kinematic distance corresponding to +23 km s^{-1} is 8.2 kpc using the rotation curve of Brand & Blitz (1993), who adopt $R_0 = 8.5$ kpc and $\Theta_0 = 220 \text{ km s}^{-1}$. This is consistent with the distance derived from the pulsar DM. We adopt 8 kpc as

the distance to G54.1+0.3 and the IR loop, and note that this is the distance to the Perseus spiral arm in this direction.

5. POST MAIN-SEQUENCE TRIGGERED STAR FORMATION?

The alignment of the YSOs along a small, loop-like structure strongly suggests that we are observing star formation triggered by some mechanism originating at the center. It cannot be the SNR G54.1+0.3, however, because the remnant is only a few thousand years old. Instead, the location of the G54.1+0.3 pulsar near the center of the IR loop indicates that it is most likely the progenitor star of the SNR and that the massive progenitor star produced an HII region/wind bubble that compressed the ambient medium into a shell that fragmented and collapsed to form the YSOs.

What is more interesting about this system is that the triggered star formation must have occurred near the end of the progenitor’s life, possibly when it was in its post main-sequence phase. The ages of early Herbig Be stars are not well known because they usually cannot be estimated from the H-R diagram (e.g., Testi, Palla, & Natta 1998). The surrounding diffuse emission in the IR loop, which might be the emission from dust grains in natal cloud heated either by the YSOs or/and other nearby B stars, indicates that they are young. We can set a limit on the age of the YSOs by noting that 100 M_{\odot} of stars in a region with a radius of 2 pc should have a 1D velocity dispersion of about 0.2 km s^{-1} . In order for these stars to have a regular spacing of about 0.7 pc as observed, they could not have moved more than ~ 0.35 pc, which sets a limit on their age of about 2 Myr. This limit is significantly shorter than the main-sequence lifetime of the progenitor star: Chevalier (2005) identified G54.1+0.3 as the remnant of Type IIP SN, with a progenitor mass $\sim 10 - 25 M_{\odot}$. The destructive impact of a massive star on the ambient molecular cloud increases rapidly with stellar mass (Chevalier 1999), so the small size of the IR loop and the regular structure seen in the spatial distribution of the YSOs suggest that the progenitor was near the lower end of this mass range. A 15 M_{\odot} star has a lifetime ~ 13 Myr, and it spends about 10% of its life in the post main-sequence phase (Schaller et al. 1992). The post main-sequence lifetime increases for lower stellar masses. Therefore, it is possible that the YSOs formed during the post main-sequence phase, although it is likely that the progenitor had a significant dynamical effect on the natal cloud while it was still on the main sequence.

We do not have enough information to determine why the triggering was delayed, i.e., why it did not occur during the first few Myr as theories predict (e.g., Hosokawa & Inutsuka 2006). Two possibilities can be ruled out: The triggering was most likely not due to the wind associated with the red supergiant (RSG) phase of evolution, since a typical RSG wind is far too weak to have a significant effect on the shell (Chevalier & Emmering 1989). In any case, the RSG wind in G54.1+0.3 may have been particularly weak since no SNR shock propagating into ambient or circumstellar medium has been detected (Chevalier 2005). One might also think that the temperature and ionization of the ambient molecular gas would drop signif-

icantly when the progenitor evolved off the main sequence, but Spaans et al. (1994) showed that the temperature and ionization in molecular gas that is near a star do not vary much for effective temperatures in the range $(6 - 30) \times 10^3$ K. A potential explanation for the delay in the triggering of the star formation is that the natal cloud was shielded by other material until a few Myr ago, when it was exposed to the star by a combination of motion of the star relative to the cloud and photoevaporation of the intervening gas. Future observations will reveal the properties of the newly formed stars and shed light on the triggering of star formation by evolved stars.

This work is based in part on observations with *AKARI*

, a JAXA project with the participation of ESA, and also in part on observations made with the *Spitzer Space Telescope*, which is operated by the Jet Propulsion Laboratory, California Institute of Technology under a contract with NASA. We wish to thank David Hollenbach and Stan Kurtz for their helpful comments. This work was supported by the Korea Science and Engineering Foundation (R01-2007-000-20336-0) and the Korea Research Foundation (R14-2002-058-01003-0). The research of CFM is supported by the National Science Foundation through grants AST-0606831 and PHY05-51164. This publication makes use of molecular line data from the Boston University-FCRAO Galactic Ring Survey (GRS).

REFERENCES

- Bessell, M. S. & Brett, J. M. 1988, *PASP*, 100, 1134
 Brand, J., & Blitz, L. 1993, *A&A*, 275, 67
 Camilo, F., Lorimer, D. R., Bhat, N. D. R., Gotthelf, E. V., Halpern, J. P., Wang, Q. D., Lu, F. J., & Mirabal, N. 2002, *ApJ*, L71
 Castelli, F. & Kurucz, R. L. 2003, in *IAU Symp. Ser. 210* edited by N. Piskunov, W.W. Weiss, & D.F. Gray, 20
 Chevalier, R. A. 1999, *ApJ*, 511, 798
 Chevalier, R. A. 2005, *ApJ*, 619, 839
 Chevalier, R. A., & Emmering, R. T. 1989, *ApJ*, 342, L75
 Draine, B. T. 2003, *ARAA*, 41, 241
 Elmegreen, B. G. 2002a, in *IAU Symp. Ser. 207* edited by D. Geisler, E. K. Grebel, & D. Minniti, 390
 Hillenbrand, L. A., Strom, S. E., Vrba, F. J., & Keene, J. 1992, *ApJ*, 397, 613
 Hosokawa, T. & Inutsuka, S.-I. 2006, *ApJ*, 646, 240
 Jackson, J. M., et al. 2006, *ApJS*, 163, 145
 Lu, F. J., Wang, Q. D., Aschenbach, B., Durouchoux, P., & Song, L. M. 2002, *ApJL*, 568, 49L
 Malfait, K., Bogaert, E., & Waelkens, C. 1998, *A&A*, 331, 211
 Martins, F., Schaerer, D., & Hillier, D. J. 2005, *A&A*, 436, 1049
 Muzerolle, J. et al. 2004, *ApJS*, 154, 379
 Nakajima, Y. 2005, *AJ*, 129, 776
 Onaka, T. et al. 2007, *PASJ*, 59, S401
 Schaller, G., Schaerer, D., Meyner, G., & Maeder, A. 1992, *A&AS*, 96, 269
 Schmidt-Kaler, T. 1982, in *Landoldt-Börnstein, New Series Group, VI, Vol. 2*, ed. K. Schaifers, & H. H. Voigt (Berlin: Springer-Verlag), 1
 Slane, P. 2007, preprint (arXiv: 0711.1002)
 Spaans, M., Tielens, A.G.G.M., van Dishoeck, E. F., & Bakes, E.L.O. 1994, *ApJ*, 437, 270
 Stil, J. M., Taylor, A. R., Dickey, J. M., Kavars, D. W., Martin, P. G., Rothwell, T. A., Boothroyd, A. I., Lockman, F. J., & McClure-Griffiths, N. M. 2006, *AJ*, 132, 1158
 Testi, L., Palla, F., & Natta, A. 1998, *A&AS*, 133, 81
 Velusamy, T. & Becker, R. H. 1988, *AJ*, 95, 1162
 Zinnecker, H. & Yorke, H. W. 2007, *ARAA*, 45, 481

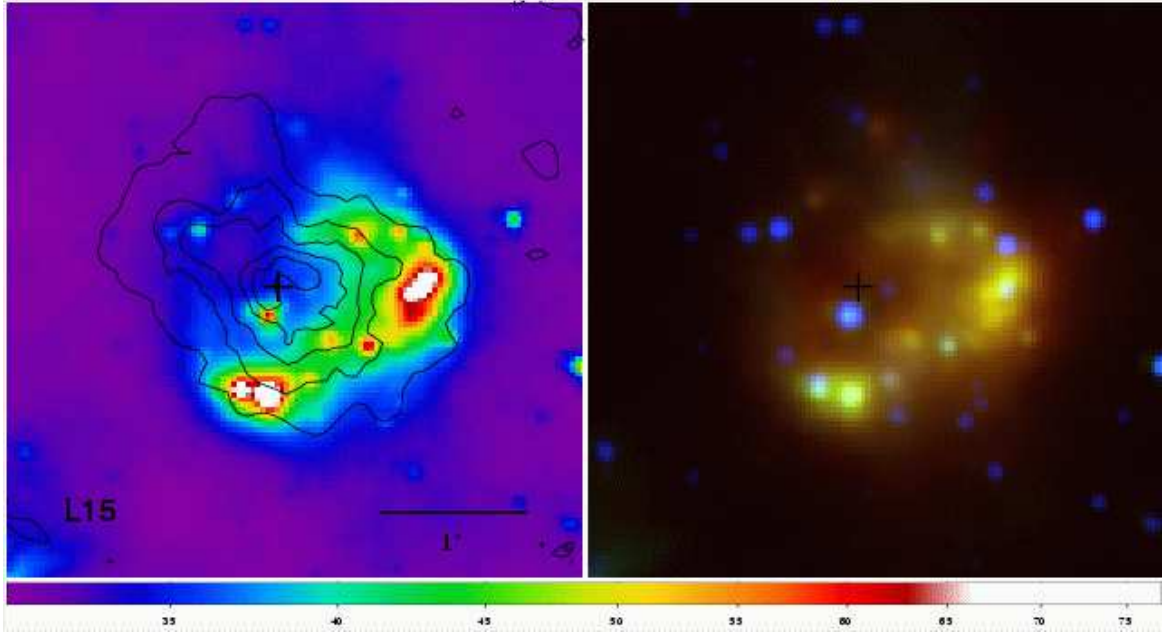


FIG. 1.— (left) *AKARI* 15 μm image of the SNR G54.1+0.3. The cross marks the position of the pulsar at $(\alpha_{2000}, \delta_{2000}) = (19^{\text{h}}30^{\text{m}}30^{\text{s}}.13, +18^{\circ}52'14.''1)$. VLA 4.85 GHz radio contours are overlaid. The contour levels are equally spaced at every 1.28 K from 0.22 K in brightness temperature. Contour levels increase toward the center of the SNR. The scale bar corresponds to $1'$ or 2.3 pc at 8 kpc. The color bar is given at the bottom of the image in units of MJy sr^{-1} . North is up and east is to the left. (right) Three-color image generated from the *Spitzer* IRAC 5.8 μm (B), the *AKARI* 15 μm (G), and the *Spitzer* MIPS 24 μm (R).

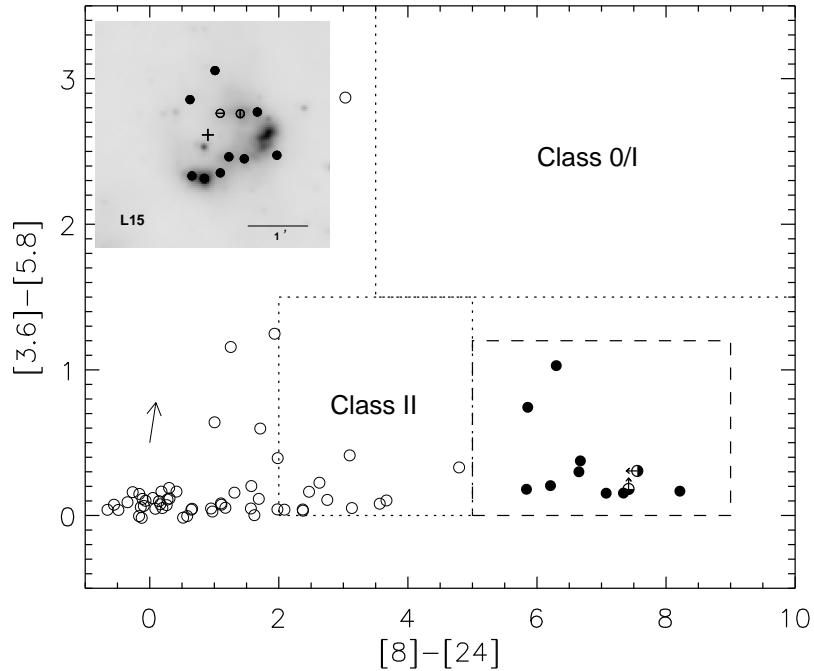


FIG. 2.— *Spitzer* color-color diagram for 64 MIR sources detected in the IRAC and MIPS 24 μm bands with a [24] magnitude error less than 0.2 mag. The sources along the IR loop are well defined in this diagram by their strong [8]–[24] excess and moderate or small [3.6]–[5.8] excess, i.e., $5 < [8] - [24] < 9$ and $0 < [3.6] - [5.8] < 1.2$. The sources within this box are marked by solid dots. (See the text for an explanation of half-filled dots.) The areas occupied by class 0/I and class II sources determined from previous studies are shown as dotted lines. The arrow is a reddening vector of $A_V = 10$. The inset shows the distribution of the sources within the dashed box on the *AKARI* 15 μm image.

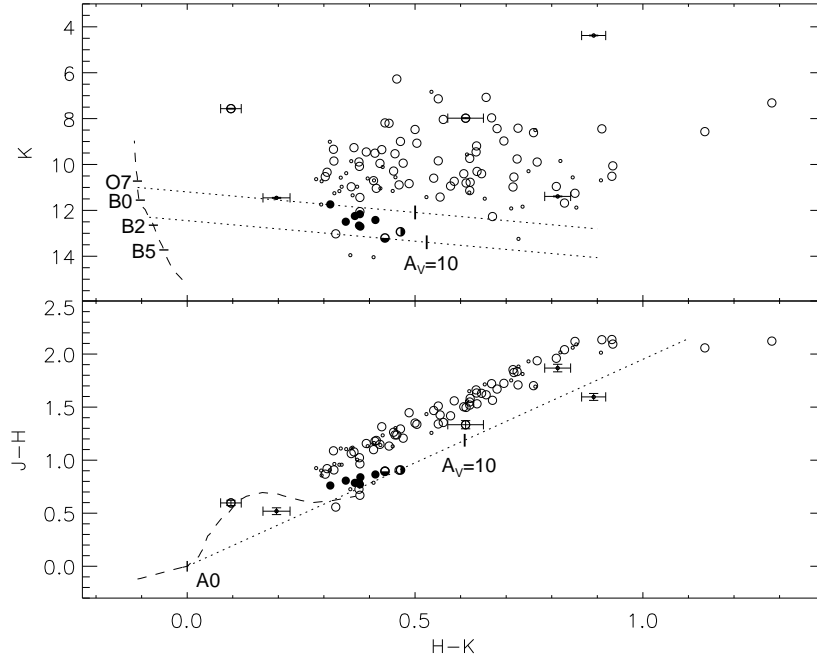


FIG. 3.— The 2MASS JHK_s color-color and color-magnitude diagrams for all 110 MIR sources identified in the 2MASS JHK_s bands. The small dots represent sources not detected in either *Spitzer* MIPS or IRAC bands while the other symbols have the same meaning as in Fig. 2. The dashed line represents the MS. In the color-color diagram, the dotted line represents interstellar reddening line of A0 star. Along the reddening line, the position at which $A_V = 10$ is marked. In the color-magnitude diagram, the dashed line with spectral types represents the MS at a distance of 8 kpc. The dotted lines represent the reddening lines that bound the YSOs. Note that the YSOs (solid dots) are clustered around the positions of reddened B1.5–O8 stars.

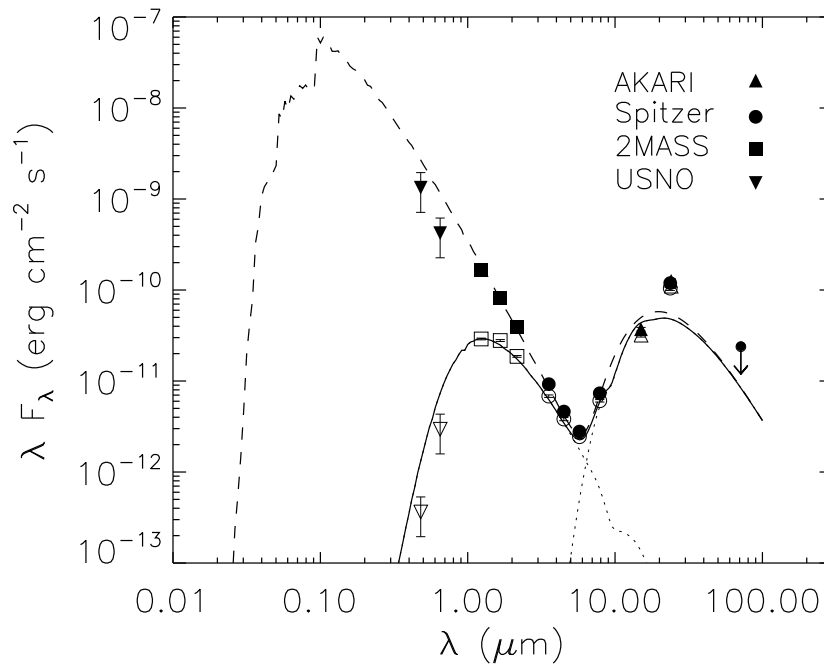


FIG. 4.— SED of the most luminous YSO in the K_s band. The open symbols represent observed fluxes while the filled symbols represent extinction-corrected fluxes. The *Spitzer* $70 \mu\text{m}$ flux is an upper limit. The dashed line is a model SED composed of a stellar emission at $T_* = 35,000 \text{ K}$ and a black body at 190 K . The solid line shows the reddened SED and the dotted lines their individual components.